Crustal structure of the Mid Black Sea High from wide-angle seismic data

D. J. Shillington[1], T. A. Minshull[2], R. A. Edwards[3] and N. White[4]

[1] Lamont-Doherty Earth Observatory, 61 Route 9W, Palisades, NY10964, USA; djs@ldeo.columbia.edu

[2] Ocean and Earth Science, National Oceanography Centre Southampton, University of Southampton, European Way, Southampton SO14 3ZH, UK; tmin@noc.soton.ac.uk

[3] National Oceanography Centre, European Way, Southampton SO14 3ZH, UK; r.edwards@edwardsgeo.co.uk

[4] Bullard Laboratories, University of Cambridge, Madingley Road, Cambridge CB3 0EZ; nwhite@esc.cam.ac.uk

Abstract

The Mid Black Sea High comprises two en-echelon basement ridges, the Archangelsky and Andrusov Ridges that separate the western and eastern Black Sea basins. The sediment coverage above these ridges has extensive seismic reflection coverage, but the crustal structure beneath is poorly known. We present results from a densely sampled wide-angle seismic profile, coincident with a pre-existing seismic reflection profile, which elucidates the crustal structure. We show that the basement ridges are covered by c. 1-2 km of pre-rift sedimentary rocks. The Archangelsky Ridge has higher pre-rift sedimentary velocities and higher velocities at the top of basement (~6 km/s). The Andrusov Ridge has lower pre-rift sedimentary velocities and velocities less than 5 km/s at the top of the basement. Both ridges are underlain by c. 20-km thick crust with velocities reaching c. 7.2 km/s at their base, interpreted as thinned continental crust. These high velocities are consistent with the geology of

the Pontides, which is formed of accreted island arcs, oceanic plateaux and accretionary complexes. The crustal thickness implies crustal thinning factors of ~1.5-2. The differences between the ridges reflect different sedimentary and tectonic histories.

Introduction

Several episodes of extension and shortening have shaped the Black Sea region since Permian times [e.g., *Nikishin et al.*, 2003; *Robertson et al.*, 2004; *Yilmaz et al.*, 1997], which led to the addition of a series of volcanic arcs, oceanic plateaux and accretionary complexes to the Eurasian margin [e.g., *Okay et al.*, 2013]. The basin is thought to have formed in a back-arc extensional environment because of its close spatial association with the subduction of both the Paleo- and Neo-Tethys Oceans [e.g., *Letouzey et al.*, 1977], but the timing and style of this opening history remain controversial, partly because the thick sediment coverage means that the oldest sedimentary fill has not been drilled [*Banks et al.*, 1997; *Nikishin et al.*, 2015a; *Okay et al.*, 1994; *Zonenshain and Le Pichon*, 1986; *Okay et al*., this volume]. The Black Sea is commonly subdivided into eastern and western basins; these sub-basins are separated by the Mid Black Sea High (MBSH), a system of buried basement ridges that runs SW-NE [Fig. 1; e.g., *Nikishin et al.*, 2015b; *Okay et al.*, 1994].

The opening of the western basin may be estimated from the ages of arc volcanic rocks in the western Pontides and from associated plate reconstructions; this evidence suggests a Middle to Upper Cretaceous age [*Görür*, 1988; *Okay et al.*, 1994; *Okay et al.,* this volume]. Based on seismic refraction and gravity data, the crust in the centre of the basin is 7-8 km thick and has velocities consistent with the presence of oceanic crust, suggesting that rifting culminated in seafloor spreading [*Belousov et al.*, 1988; *Letouzey et al.*, 1977; *Starostenko et al.*, 2004].

The age and nature of the eastern basin are more controversial. The basin is thought to have formed by rotation of the Shatsky Ridge relative to the Mid Black Sea High [Figs. 1 and 2; *Nikishin et al.*, 2003; *Okay et al.*, 1994]. The main phase of opening has been interpreted as Jurassic, Cretaceous [*Nikishin et al.*, 2003; *Nikishin et al.*, 2015a; *Okay et al.*, 1994; *Zonenshain and Le Pichon*, 1986], Early Eocene/Paleocene [*Banks et al.*, 1997; *Robinson et al.*, 1995; *Shillington et al.*, 2008], or Eocene [*Kazmin et al.*, 2000; *Vincent et al.*, 2005]. Based on gravity and early seismic data, the crust in the centre of this basin was inferred to have a thickness of ~10-11 km and seismic velocities are lower than those of typical oceanic crust, suggesting the presence of thinned continental crust [*Belousov et al.*, 1988; *Starostenko et al.*, 2004]. However, results from a wide-angle seismic experiment in 2005 suggest that the crustal structure varies along the basin, with the western part floored by thinned continental crust (7-9 km thick), and thicker, higher velocity crust below the eastern part that is attributed to magmatically robust early seafloor spreading resulting in early oceanic crust that is thicker and has higher velocities than average oceanic crust [*Shillington et al.*, 2009].

The Mid Black Sea High itself is divided into the en-echelon Archangelsky and Andrusov ridges, which have different sediment thicknesses and are inferred to have different structure and origin [*Nikishin et al.*, 2015b; *Robinson et al.*, 1996] (Fig. 1b). These ridges are poorly explored compared to the basins either side. The Andrusov

Ridge is inferred to have formed during early opening of the eastern basin [*Nikishin et al.*, 2015a; *Okay et al.*, 1994; *Robinson et al.*, 1996]. This rifting event is inferred to have been amagmatic in this part of the basin [*Shillington et al.*, 2009]. Alternatively, the Andrusov Ridge is interpreted as a marginal ridge associated with the opening of the western basin along the West Crimean transform fault [*Tari et al.*, 2015]. The Archangelsky Ridge was formed by the opening of the Sinop Trough, which is linked to the western basin and is interpreted to have opened in Cretaceous to Palaeocene times [*Espurt et al.*, 2014; *Robinson et al.*, 1996], with ongoing extension into the Miocene [*Espurt et al.*, 2014; *Rangin et al.*, 2002]. An Upper Cretaceous sedimentary sequence and lower Cretaceous platform carbonate rocks have been dredged where the pre-rift sequences outcrops on the flank of Archangelsky Ridge, providing an upper limit on its age of formation [*Rudat and Macgregor*, 1993; *Robinson et al.* 1996].

After their formation, both ridges have also experienced compressional deformation [*Espurt et al.*, 2014; *Rangin et al.*, 2002]. This region has likely experienced multiple episodes of compression, continuing to the present; apatite fission track data and paleostress measurements onshore show that inversion of rifting structure onshore occurred as early as 55 Ma [*Saintot & Angelier,* 2002; *Espurt et al.,* 2014] following extension leading to opening of eastern Black Sea. Active compression continues around margins of easternmost Black Sea today based on seismicity and onshore geology, particularly in the Caucaus [*Saintot & Angelier,* 2002; *Gobarenko et al.* 2016].

Published constraints on crustal structure beneath the ridges are sparse. Seismic refraction data acquired in the 1960s were recently re-analysed using more modern ray-tracing techniques [*Yegorova and Gobarenko*, 2010]. This analysis suggests a crustal thickness of c. 20 km beneath both ridges and crustal velocities in the range 6.0-7.0 km/s, interpreted as representing thinned continental crust. A more modern profile crossing the southern part of Archangelsky Ridge suggests that here, crustal thickness reaches c. 25 km [*Shillington et al.*, 2009]. In this paper we present results from a modern, densely sampled wide-angle seismic profile that crosses the Andrusov Ridge close to its southern tip and the Archangelsky Ridge at its northern tip (Fig. 1).

Wide-Angle Seismic Data

An onshore-offshore wide-angle seismic dataset was collected in 2005 using the R/V *Iskatel* to determine the deep structure of the eastern basin and Mid Black Sea High. Seventeen four-component short-period ocean-bottom seismometers (OBSs) from GeoPro were deployed on Profile 4 across the Andrusov Ridge (Fig. 1; Table 1), and they recorded seismic shots generated from an airgun array with a total volume of 3140 in^3 that was triggered every 90 s (shot spacing c. 150 m). Profile 4 was co-located with existing industry seismic reflection data, 91-106 (Figs. 1 and 2).

Data Analysis

Data processing

Water-wave arrivals were used to relocate OBS positions on the seafloor, using a seafloor depth determined by echosounder at the position of each deployment and a water velocity of 1.47 km/s. Relocated positions were typically less than 75 m from deployment positions, but three OBS have relocated positions that differ by 200-300 m from deployment positions. We applied a minimum phase band-phase filter with corners at 3, 5, 15, 20 Hz to suppress noise, and applied offset dependent gains and a reduction velocity of 8 km/s.

Phase identification

We identified refractions and wide-angle reflections from the pre-rift sedimentary section, the crust and the upper mantle that could be consistently identified on a majority of the receiver gathers. Phase interpretations and velocity models of the overlying syn- and post-rift sedimentary section have been presented elsewhere [*Scott et al.*, 2009]. Travel-time picks were made manually of the following phases: reflections off the base of an interpreted pre-rift sedimentary layer (PprP), crustal refractions (Pg), reflections from the base of the crust (PmP), and upper mantle refractions (Pn) (Fig. 3; Table 2). Reflections from the base of the interpreted pre-rift sedimentary section are observed from near-vertical incidence to offsets up to ~30 km and have picking uncertainties of 30-50 ms. Crustal refractions are observed as first arrivals at offsets from ~12-100 km and have picking uncertainties of 30 to 75 ms. Reflections from the base of the crust are observed at offsets between ~35-100 km; the offsets where PmP reflections are observed vary significantly over the line, indicating variations in crustal thickness. Likewise, the amplitude and character of PmP reflections is also highly variable and thus picks of this phase have relatively high uncertainties of 125 ms. We observed limited and relatively low amplitude refractions interpreted to arise from the upper mantle in some receiver gathers; these refractions are weak and variable, and have a picking uncertainty of 125 ms. Figure 3 shows examples of OBS data, phase identifications, and associated ray paths.

Wide-angle reflections interpreted to originate from the base of the interpreted pre-rift sedimentary layer can be linked to a coincident industry seismic reflection profile (BP91-106, Fig. 2). Picks of this interface were thus also made on the reflection profile (Fig. 2, red dotted line) and included in the inversion. We assigned an uncertainty of 100 ms to these picks to account for uncertainties in associating MCS and wide-angle reflections and for small-scale variations in interface geometry that cannot be recovered by inversion.

Velocity modelling

The travel-time picks described above were used to invert for velocities of the pre-rift sedimentary section, crust and upper mantle. We used JIVE3D, a regularized tomographic inversion code [*Hobro et al.*, 2003], which solves for a minimum structure layer-interface model that fits the data within its uncertainties. Velocities within each layer and interface depths are defined by splines and vary smoothly; interfaces represent velocity discontinuities. The forward problem involves tracing a fan of rays from each OBS position through specified layers in the model to generate predicted travel times (i.e., ray shooting); the ray that arrives within a distance tolerance of the target with the minimum travel time is used. Inversion involves a sequence of linear steps to reduce the difference between observed and predicted travel times (e.g., Figs. 4d and 5d) and satisfy other smoothing criteria. In each step, smoothing is reduced and structure is allowed to develop to improve data fit. Smoothing is implemented during inversion by minimizing a function of data misfit and model roughness.

We employed a layer stripping approach for this line. The previously determined velocity structure of the post- and syn-rift sediment from *Scott et al.* [2009] was held fixed. We first inverted for the interpreted pre-rift sediment layer using picks of wide-angle reflections from OBS data and vertically-incident reflections from the coincident seismic reflection profile (Fig. 2). This layer was then held fixed during the inversion for crustal and upper mantle structure. The inversion converged more quickly and stably for both the pre-rift sedimentary section and for the crustal/mantle sections when we inverted for them separately. However, inverting for all layers simultaneously yielded the same overall velocity structure. We also performed two different inversions for crust/mantle structure. The first inversion used only first arriving refractions from the crust and mantle. The second inversion included interpreted wide-angle reflections from the base of the crust (PmP) in addition to the first arrivals. The purpose of performing two inversions for the crust and upper mantle structure was to assess which features in the model arise from the inclusion of wide-angle reflections from the base of the crust; identifying PmP is associated with more uncertainty and subjectivity than first arrivals. We are most confident of features that are present in both the first-arrival and reflection/refraction tomographic inversions, and more cautious of features that are primarily constrained by the PmP reflections.

We used a grid spacing of 1 km x 0.5 km in the pre-rift interval, and 1x1 km in the crust and upper mantle. For both inversions, we applied twice as much horizontal smoothing than vertical smoothing and allowed more interface roughness than velocity roughness. A simple 1D velocity model and constant interfaces were used for the starting models in both inversions.

The inversion for the pre-rift layer used 825 picks from the OBS data and 129 picks from the MCS data. The final model has a chi-squared misfit of 1.29 and RMS residual of 72 ms if only the OBS picks are included. Larger misfits are associated with the MCS picks since they include smaller scale variations in interface geometry than can be recovered by the inversion. If these are included, the overall chi-squared misfit is 1.65, and the RMS residual is 90 ms.

The first-arrival inversion for the crust and upper mantle structure used 5732 picks. The final model has a chi-squared value of 0.96 and an RMS residual of 76 ms. The reflection/refraction inversion used 7085 picks. The final model has a chi-squared value of 2.23 and an RMS residual of 127 ms.

Based on ray coverage, data fit and testing of different inversion parameterizations, we discuss the confidence that should be placed in different features of our final models. The upper crustal structure is very well sampled by ray coverage associated with our travel-time picks, and refractions from this part of the model have relatively low misfits (Figs. 3-5). Similar features are apparent in both the reflection/refraction tomography and the first-arrival tomography. Thus, we consider the variations in upper crustal velocity structure between the Andrusov and Archangelsky Ridge to be a robust result (Figs. 4b and 5b). The lowermost crustal sections beneath the Andrusov and Archangelsky ridges are only constrained by sparse turning wave coverage and relatively sparse reflections from the base of the crust (Figs. 3 and 5). Because the uppermost part of the lower crust is sampled by reversed refracted arrivals, we are confident that high velocities are required. However, we cannot constrain the velocity gradient of the lowermost crust or absolute velocity at the very base of the lower crust, and there are thus tradeoffs between velocities in the lowermost crust and depth to the base of the crust. Both wide-angle reflections and vertically incident reflections constrain the interpreted pre-rift sedimentary layer on top of the MBSH. We find relatively high data misfits for phases defining this layer (Table 2), which we attribute to substantial lateral variability that cannot be accounted for in the analysis of OBS spaced at ~15 km. However, we think that the large-scale patterns of thickness and velocity are well constrained.

Although we obtained an excellent misfit for the first-arrival tomography model (chi-squared value of 0.96), our favored model from reflection/refraction tomography has a higher chi-squared value of 2.23. We relaxed the data misfit criteria to obtain a relatively smooth model; models with better data fit were substantially rougher. We feel this choice is justified by the likely three-dimensionality of velocity structure beneath these complex ridges and the complexity of sedimentary, crustal and upper mantle phases observed on OBS.

Results and Discussion

The final velocity models across the Mid-Black Sea High provide constraints on the deep sedimentary and crustal structure of this composite ridge.

Sedimentary rocks overlying the Mid Black Sea High

The flat-lying post-rift sedimentary rocks exhibit a low-velocity zone in the Miocene Maikop formation (Figs. 5 and 6) that extends across the eastern basin and also appears to be present above parts of the MBSH and in the Sinop Trough [Fig. 6; *Scott et al.*, 2009]. The low-velocity zone is attributed to fluid overpressure, and fluid pressures close to lithostatic have been inferred [*Scott et al.*, 2009], though application of a more sophisticated approach in the eastern basin [*Marin-Moreno et al.*, 2013a; b] suggests that fluid pressures are lower than those derived from the empirical approaches of *Scott et al.* [2009].

Wide-angle reflections in the OBS data (Fig. 3) and reflections in the reflection profile (Fig. 6) define a distinct layer with a thickness of 1-2 km and velocities of 3.0-4.75 km/s on top of the Andrusov and Archangelsky Ridges (Fig. 5). Based on the character of this layer in the reflection profile, dredging on the Archangelsky Ridge and drilling of the Andrusov Ridge, we interpret this layer to represent a sequence of prerift Upper Cretaceous sedimentary rocks [*Rudat & McGregor,* 1993; *Aydemir & Demirer*, 2013]. This layer is characterized by brightly reflective layering in the reflection profile, which is consistent with a sedimentary origin (Figs. 2, 6). Drilling on Andrusov Ridge at Sinop-1 recovered a relatively thin layer of Upper Cretaceous carbonate rocks [*Aydemir & Demirer,* 2013]. Aydemir & Demirer [2013] suggest that the thickness of this interval would be strongly controlled by basement topography at the time of deposition and thus be highly variable, which may explain why we appear to observe a thicker Upper Cretaceous layer on Profile 4. A similar sequence overlies the Shatsky Ridge to the north [Fig. 1; *Nikishin et al.*, 2015b; *Robinson et al.*, 1996].

The base of this layer is marked by a bright, continuous reflection in the reflection profile (Fig. 6), which has been interpreted to mark the top of Lower Cretaceous platform carbonate rocks [*Rudat & McGregor,* 1993; *Robinson et al.*, 1996]. Based on dredging results on the shallow part of the Archangelsky ridge, we interpret the uppermost basement beneath this reflection as being composed of Lower Cretaceous platform carbonate rocks and other older prerift sedimentary rocks. Platform carbonate rocks are expected to have similar P-wave velocities to upper crystalline crust [*Christensen & Mooney,* 1995], so it is not possible for us to definitely identify carbonate rocks or quantify their thickness, but the nearby dredging results suggest prerift sedimentary rocks are likely present in the uppermost basement here. The uppermost basement beneath the prominent reflection described above reaches 6-6.25 km/s beneath the top of the Archangelsky Ridge, and drops to c. 4.5 km/s beneath the Andrusov Ridge. The overlying layer interpreted to represent Upper Cretaceous prerift sedimentary rocks also has significantly higher velocities beneath Archangelsky Ridge than beneath Andrusov Ridge. These differences may be attributed to several factors. First, although Archangelsky Ridge is generally a shallower feature (Fig. 1), at the location of Profile 4 it is more deeply buried, so the pre-rift sedimentary rocks may have undergone greater compaction and diagenesis. Secondly, seismic reflection data suggest that the Andrusov Ridge is disrupted by more faults than the Archangelsky Ridge [*Robinson et al.,* 1996], and fracturing associated with these faults may reduce the velocity by creating zones of higher porosity and/or causing an elongation of pores, which have a bigger impact on elastic properties [*Töksöz et al*., 1976] . Thirdly, other differences in lithology may contribute to observed variations in velocity. Finally, the low-velocity layer in the post-rift directly abuts the Andrusov Ridge, but is separated from Archangelsky Ridge by a layer of higher-velocity material. Therefore it is possible that fluid overpressure is transmitted into pre-rift sedimentary rocks on the Andrusov Ridge but not on the Archangelsky Ridge.

Crustal structure and Implications for Tectonic Evolution

The Andrusov and Archangelsky Ridges exhibit distinctly different crustal velocity structures. As described in the previous section, the Archangelsky Ridge has higher velocities in the uppermost basement (6-6.25 km/s) and a relatively low velocity gradient (~0.075 km/s/km). In contrast, the Andrusov ridge has velocities in the shallow basement as low as 4.5 km/s and a high velocity gradient in the upper 10 km of 0.25 km/s/km. These differences might be associated with different degrees of fracturing of platform carbonate rocks (see previous section) or of crystalline rocks, or might arise because the prerift sedimentary sequence within the basement is thicker beneath Andrusov Ridge, as perhaps suggested by seismic reflection data (Fig. 2).

Beneath both ridges, the velocity gradient is reduced in the lower crust, and velocities reach a maximum of 7.2-7.3 km/s at the base of the crust (Fig. 5). These velocities are somewhat higher than those observed beneath Archangelsky Ridge on Profile 3 (~6.75-7 km/s) [*Shillington et al.*, 2009] (Fig. 1), and may indicate the presence of a more mafic pre-rift crust [e.g., *Christensen and Mooney*, 1995]. Rifting to form the eastern Black Sea occurred in a series of terranes accreted to the Euroasian margin, which include volcanic arcs and oceanic plateaux, both of which are typified by high-velocity lower crust in modern analogues [*Calvert*, 2011; *Kodaira et al.*, 2007; *Shillington et al.*, 2004].

These velocities are also only slightly lower than lower-crustal velocities observed in crust within the centre of the eastern part of the Eastern Basin [*Shillington et al.*, 2009], which were interpreted as evidence for new magmatic crust formed during magma rich rifting and early spreading. However, the relationship between lower crustal velocity and crustal thickness suggests that synrift magmatism is not responsible for the high lower crustal velocities beneath the MBSH. In the eastern part of the Eastern Basin [*Shillington et al.*, 2009] and at other volcanic rifted margins worldwide [e.g., *Holbrook and Kelemen*, 1993; *White et al.*, 2008], high-velocity lower crust (~7.4-7.5 km/s) interpreted to represent mafic synrift intrusions is most prominent in the area of crustal thinning. In contrast, the highest velocities observed beneath the MBSH occur in the thickest crust and do not increase towards the thinned margins of the ridge. Consequently, we propose that high lower crustal velocities beneath the MBSH represent high velocities associated with accreted volcanic arcs and oceanic plateaux in the pre-rift crust. Hence our observations from Profile 4 is consistent the view that extension in the western part of the eastern Black Sea Basin was largely amagmatic [*Shillington et al.*, 2009].

The crustal layer, that may include platform carbonate rocks and possibly other pre-rift sedimentary rocks, thickens beneath both ridges to reach a maximum of 20-23 km (Fig. 5). Between the two ridges, it decreases to c. 16 km, providing evidence that the modest increase in sediment thickness between the two ridges (Fig. 1) is associated with crustal-scale extension. Although the Archangelsky Ridge is deeply buried at the location of Profile 4 (Fig. 1), it clearly remains a major crustal feature at this location. Uppermost mantle velocities are a little below 8 km/s. Based on teleseismic receiver functions, gravity data and limited wide-angle seismic constraints, the crustal thickness onshore Turkey in the vicinity of Archangelsky Ridge is c. 35 km [*Ozacar et al.*, 2010; *Yegorova et al.*, 2013], with thicker crust farther east where it is affected more by compressional deformation. Therefore the crust along Profile 4 has been thinned by a factor of 1.5-2. The degree of thinning is somewhat lower than inferred by *Shillington et al.* [2008] based on the relationship between sediment thickness and thinning factor on a well-constrained profile; this relationship gives a thinning factor of 2-2.5 along most of Profile 4 (Fig. 7). One possible explanation for this difference is that the "crust" of the Mid Black Sea High may include sections of pre-rift sedimentary rocks that are not a part of the unthinned crustal section onshore [*Okay et al*, this volume].

Conclusions

From our analysis of data from a wide-angle seismic profile across the Mid Black Sea High, comprising the en echelon Archangelsky and Andrusov ridges, we conclude that:

1. The basement highs are covered by at least 1-2 km layer of pre-rift sedimentary rocks overlying a higher-velocity basement that may include pre-rift sedimentary rocks, including platform carbonates that cannot be readily distinguished from underlying crystalline crust.
2. The pre-rift sedimentary rocks and upper basement have higher velocities on the Archangelsky Ridge and lower velocities on the Andrusov Ridge. These differences could be explained by different amounts of faulting or changes in the abundance and/or composition of prerift sedimentary rocks.
3. The lower crust has a low velocity gradient and velocities exceed 7.0 km/s at its base; the velocity structure is consistent with the presence of a mafic pre-rift crust with little magmatic addition during rifting.

4. The crust is 20-23 km thick beneath the ridges and c. 16 km thick between them, representing thinning factors of 1.5-2.0 compared to adjacent crust in northeastern Turkey.

Acknowledgments

We thank T. Besevli, G. Coskun, A. Demirer, M. Erduran, S. Jones, R. O'Connor, B. Peterson, A. Price, K. Raven, and M. Shaw-Champion and the officers, crew and technical team aboard *R/V Iskatel* for their support during the acquisition and analysis of this dataset. This work was supported by the Natural Environment Research Council (UK) (NER/T/S/2003/00114 and NER/T/S/2003/00885), BP and the Turkish Petroleum Company (TPAO). BP and TPAO generously provided access to the seismic reflection data. We also thank N. Hodgson and an anonymous reviewer for constructive comments that greatly improved the manuscript.

Figure Captions

Figure 1. a. Elevation/bathymetry of Black Sea region from GEBCO showing the location of 2005 onshore/offshore seismic refraction experiment. Shot lines are indicated with white lines, OBS are shown with white circles and seismometers deployed onshore shown with white triangles. OBS from Line 4, which are used in this study, are indicated with solid circles. Major tectonic elements indicated with dashed yellow lines [*Zonenshain and Le Pichon*, 1986]. Black box indicates area shown in Figure 1b. **b.** Close-up of Mid Black Sea High showing sediment thickness [*Shillington et al.*, 2008] and OBS locations from 2005 experiment. Note that Mid-Black Sea High separates the Western and Eastern basins of the Black Sea and comprises two ridges: the Archangelsky Ridge and the Andrusov Ridge. Seismic reflection profile 91-106 (Fig. 2) is shown with thick white line. It is coincident with Profile 4 but shorter; it extends southwest to between OBS 3 and 4.

Figure 2. a. Seismic reflection profile 91-106 across the Mid-Black Sea High, which is coincident with the Line 4 OBS profile (courtesy of BP and TPAO) (see Fig. 1 for location). **b.** Seismic reflection profile with interfaces used in seismic inversion. The blue, green and orange dotted lines show interpreted horizons used to invert for post- and syn-rift sedimentary structure by Scott et al. [2009]. The red dotted line shows the interpreted pre-rift sedimentary horizon used in the inversions presented here.

Figure 3. Receiver gather without picks (top panel). Data with observed picks and picking errors (closed circles and bars) and predicted picks (solid, lighter colored circles) (middle panel). Orange – PprP; Blue – Pg; Green – PmP; Red – Pn. Ray paths

through final model from reflection/refraction tomography model. **a.** OBS 2, **b.** OBS9, **c.** OBS13, **d.** OBS15.

Figure 4. **a.** Result of inversion for pre-rift sedimentary reflections (PprP) and first-arriving refractions from crust and upper mantle (Pg and Pn). Velocities contoured at 0.25 km/s. Velocity model is masked by density of ray coverage. **b.** Density of ray coverage over the velocity model in a. **c.** Observed and predicted travel-time picks. Uncertainty of observed picks indicated with bars. **d.** Travel-time residuals for picks.

Figure 5. **a.** Result of inversion for pre-rift sedimentary reflections (PprP), first-arriving refractions from crust and upper mantle (Pg and Pn), and reflections from the base of the crust (PmP). Velocities contoured at 0.25 km/s. Velocity model masked by density of ray coverage. **b.** Density of ray coverage over the velocity model in a. **c.** Observed and predicted travel-time picks. Uncertainty of observed picks indicated with bars. **d.** Travel-time residuals for picks.

Figure 6: Overlay of reflection profile 91-106 on final velocity model from reflection/refraction tomography (Fig. 5), which was converted to two-way travel time.

Figure 7: Comparison of crustal thinning factor (beta = initial thickness/rifted thickness) along Line 4 from subsidence analysis based on sediment thickness [*Shillington et al.*, 2008] and from this study assuming an initial crustal thickness of 35 km.

References

Aydemir, V., A Demirer (2013), Upper Cretaceous and Paleocene Shallow Water Carbonates along the Pontide Belt, Türkiye 19. Uluslararası Petrol ve Doğal Gaz Kongre ve Sergisi 15-17 Mayıs 2013, 284-290.

Banks, C. J., A. G. Robinson, and M. P. Williams (1997), Structure and regional tectonics of the Achara-Trialet fold belt and the adjacent Rioni and Kartli foreland basins, AAPG, Tulsa, OK.

Belousov, V. V., B. S. Volvovsky, I. V. Arkhipov, V. B. Buryanova, Y. D. Evsyukov, V. P. Goncharov, V. V. Gordienko, D. F. Ismagilov, G. K. Kislov, L. I. Kogan, V. N. Moskalenko, Y. P. Neprchnov, B. K. Ostisty, O. M. Rusakov, K. M. Shimkus, A. E. Shlenzinger, V. V. Sochelnikov, V. B. Sollogub, V. D. Solovyev, V. I. Starostenko, A. F. Starovoitov, A. A. Terekhov, I. S. Volvovsky, A. S. Zhigunov, and V. G. Zolotarev (1988), Structure and evolution of the earth's crust and upper mantle of the Black Sea, Bollettino Di Geofisica Teorica ed Applicata, 30 (117-118), 109-196.

Calvert, A. J. (2011), The Seismic Structure of Island Arc Crust, in Arc-Continent Collision, edited by D. Brown and P. D. Ryan, pp. 87-119, Springer-Verlag Berlin Heidelberg.

Christensen, N. I., and W. D. Mooney (1995), Seismic velocity structure and composition of the continental crust - a global view, Journal of Geophysical Research-Solid Earth, 100(B6), 9761-9788.

Espurt, N., J. C. Hippolyte, N. Kaymakci, and E. Sangu (2014), Lithospheric structural control on inversion of the southern margin of the Black Sea Basin, Central Pontides, Turkey, Lithosphere, 6(1), 26-34.

Gobarenko, V. S., A. V. Murovskaya, T. P. Yegorova, and E. E. Sheremet (2016), Collision processes at the northern margin of the Black Sea, *Geotectonics*, 50(4), 407-424.

Görür, N. (1988), Timing of opening of the Black Sea basin, *Tectonophysics*, *147*(3-4), 247-262.

Hobro, J. W. D., S. C. Singh, and T. A. Minshull (2003), Three-dimensional tomographic inversion of combined reflection and refraction seismic traveltime data, Geophys. J. Int., 152, 79-93.

Holbrook, W. S., and P. B. Kelemen (1993), Large igneous province on the US Atlantic margin and implications for magmatism during continental breakup, Nature, 364, 433-436.

Kazmin, V. G., A. A. Schreider, and A. A. Bulychev (2000), Early stages of evolution of the Black Sea, in Tectonics and Magmatism in Turkey and the Surrounding Area, edited by E. Bozkurt, et al., pp. 235-249, Geological Society, London.

Kodaira, S., T. Sato, N. Takahashi, A. Ito, Y. Tamura, Y. Tatsumi, and Y. Kaneda (2007), Seismological evidence for variable growth of crust along the Izu intra-oceanic arc, J. Geophys. Res., 112(B5), B05104.

Letouzey, J., B. Biju-Duval, A. Dorkel, R. Gonnard, K. Kristchev, L. Montadert, and O. Sungurlu (1977), The Black Sea: A Marginal Basin, Geophysical and Geological Data, in International Symposium of the Mediterranean Basins Split

(Yugoslavia) 25-29 October 1976, edited by B. Biju-Duval and L. Montadert, pp. 363-376, Editions Technip, Paris.

Marin-Moreno, H., T. A. Minshull, and R. A. Edwards (2013a), Inverse modelling and seismic data constraints on overpressure generation by disequilibrium compaction and aquathermal pressuring: application to the Eastern Black Sea Basin, Geophysical Journal International, 194(2), 814-833.

Marin-Moreno, H., T. A. Minshull, and R. A. Edwards (2013b), A disequilibrium compaction model constrained by seismic data and application to overpressure generation in The Eastern Black Sea Basin, Basin Research, 25(3), 331-347.

Nikishin, A. M., M. V. Korotaev, A. V. Ershov, and M.-F. Brunet (2003), The Black Sea basin: tectonic history and Neogene-Quaternary rapid subsidence modelling, Sedimentary Geology, 156, 149-168.

Nikishin, A. M., A. Okay, O. Tuysuz, A. Demirer, M. Wannier, N. Amelin, and E. Petrov (2015a), The Black Sea basins structure and history: New model based on new deep penetration regional seismic data. Part 2: Tectonic history and paleogeography, Marine and Petroleum Geology, 59, 656-670.

Nikishin, A. M., A. I. Okay, O. Tuysuz, A. Demirer, N. Amelin, and E. Petrov (2015b), The Black Sea basins structure and history: New model based on new deep penetration regional seismic data. Part 1: Basins structure and fill, Marine and Petroleum Geology, 59, 638-655.

Okay et al, THIS VOLUME

Okay, A. I., A. M. C. Sengor, and N. Görür (1994), Kinematic history of the opening of the Black Sea and its effect on the surrounding regions, Geology, 22, 267-270.

Okay, A. I., G. Sunal, S. Sherlock, D. Altiner, O. Tüysüz, A. R. C. Kylander-Clark, and M. Aygül (2013), Early Cretaceous sedimentation and orogeny on the active margin of Eurasia: Southern Central Pontides, Turkey, Tectonics, 32, 1247-1271.

Ozacar, A. A., G. Zandt, H. Gilbert, and S. L. Beck (2010), Seismic images of crustal variations beneath the East Anatolian Plateau (Turkey) from teleseismic receiver functions, in Sedimentary Basin Tectonics from the Black Sea and Caucasus to the Arabian Platform, edited by M. Sosson, et al., pp. 485-496, Geological Soc Publishing House, Bath.

Rangin, C., A. G. Bader, G. Pascal, B. Ecevitoglu, and N. Görür (2002), Deep structure of the Mid Black Sea High (offshore Turkey) imaged by multi-channel seismic survey (BLACKSIS cruise), Marine Geology, 182, 265-278.

Robertson, A. H. F., T. Ustaömer, E. A. Pickett, A. S. Collins, T. Andrew, and J. E. Dixon (2004), Testing models of Late-Palaeozoic-Early Mesozoic orogeny in Western Turkey: support for an evolving open-Tethys model, J. Geol. Soc. London, 161, 501-511.

Robinson, A. G., C. J. Banks, M. M. Rutherford, and J. P. P. Hirst (1995), Stratigraphic and structural development of the Eastern Pontides, Turkey, J. Geol. Soc. London, 152, 861-872.

Robinson, A. G., J. H. Rudat, C. J. Banks, and R. L. F. Wiles (1996), Petroleum Geology of the Black Sea, Marine Petrol. Geol., 13(2), 195-223.

Rudat, J. H., and D. S. Macgregor (1993), Unconventional exploration techniques in a high cost deep water basin: a case study from the Black Sea, Soc. of Explor. Geophys. Abstr. Progr.

Saintot, A., and J. Angelier (2002), Tectonic paleostress fields and structural evolution of the NW-Caucaus fold-and-thrust belt from Late Cretaceous to Quaternary, Tectonophysics, 357, 1-31.

Scott, C. L., D. J. Shillington, T. A. Minshull, R. A. Edwards, P. J. Brown, and N. J. White (2009), Wide-angle seismic data reveal extensive overpressures in Eastern Black Sea, Geophys. J. Int., 178, 1145-1163, doi: 1110.1111/j.1365-1246X.2009.04215.x.

Shillington, D. J., H. J. A. Van Avendonk, W. S. Holbrook, P. B. Kelemen, and M. J. Hornbach (2004), Composition and structure of the central Aleutian island arc from arc-parallel wide-angle seismic data, Geochem. Geophys. Geosys., 5(Q10006), doi:10.1029/2004GC000715.

Shillington, D. J., N. White, T. A. Minshull, G. R. H. Edwards, S. Jones, R. A. Edwards, and C. L. Scott (2008), Cenozoic evolution of the eastern Black Sea: a test of depth-dependent stretching models, Earth Planet. Sci. Lett., 265(3-4), 360-378.

Shillington, D. J., C. L. Scott, T. A. Minshull, R. A. Edwards, P. J. Brown, and N. White (2009), Abrupt transition from magma-starved to magma-rich rifting in the eastern Black Sea, Geology, 37(1), 7-10, doi:10.1130/G25302A.25301.

Starostenko, V., V. Buryanov, I. Makarenko, O. Rusakov, R. Stephenson, A. Nikishin, G. Georgiev, M. Gerasimov, R. Dimitriu, O. Legostaeva, V. Pchelarov, and C. Sava (2004), Topography of the crust-mantle boundary beneath the Black Sea Basin, Tectonophysics, 381, 211-233.

Tari, G., Schleder, Zs., Fallah, M., Turi, V., Kosi, W. and Krezsek, Cs., (2015). Regional rift structure of the Western Black Sea Basin: map-view kinematics. Transactions GCSSEPM Foundation Perkins-Rosen 34th Annual Research Conference "Petroleum Systems in Rift Basins", Houston, Texas, 372-396.

Töksöz, M. N., C. H. Cheng, and A. Timur (1976), Velocities of seismic waves in porous rocks, Geophysics, 41, 621-645.

Vincent, S. J., M. B. Allen, A. D. Ismail-Zadeh, R. Flecker, K. A. Foland, and M. D. Simmons (2005), Insights from the Talysh of Azerbaijan into the Paleogene evolution of the South Caspian region, GSA Bulletin, 117(11/12), 1513-1533.

White, R. S., L. K. Smith, A. W. Roberts, P. A. F. Christie, N. J. Kusznir, and iSIMM Team (2008), Lower-crustal intrusion on the North Atlantic continental margin, Nature, 452, 460-465.

Yegorova, T., and V. Gobarenko (2010), Structure of the Earth's crust and upper mantle of the West- and East-Black Sea Basins revealed from geophysical data and its tectonic implications, in Sedimentary Basin Tectonics from the Black Sea and Caucasus to the Arabian Platform, edited by M. Sosson, et al., pp. 23-42, Geological Soc Publishing House, Bath.

Yegorova, T., V. Gobarenko, and T. Yanovskaya (2013), Lithosphere structure of the Black Sea from 3-D gravity analysis and seismic tomography, Geophysical Journal International, 193(1), 287-303.

Yilmaz, Y., O. Tüysüz, E. Yigitbas, S. Genç, Can, and A. M. C. Sengör (1997), Geology and Tectonic Evolution of the Pontides, in Regional and petroleum geology of the Black Sea and surrounding region: AAPG Memoir 68, edited by A. G. Robinson, pp. 183-226, AAPG, Tulsa.

Zonenshain, L. P., and X. Le Pichon (1986), Deep Basins of the Black Sea and Caspian Sea as Remnants of Mesozoic Back-Arc Basins, Tectonophysics, 123, 181-211

Table 1: Relocated OBS positions

OBS	Latitude (ºN)	Longitude (ºE)
1	42.511005	35.212699
2	42.549179	35.322692
3	42.589855	35.432331
4	42.625923	35.543609
5	42.663829	35.654865
6	42.701	35.766201
7	42.738536	35.876911
8	42.777019	35.987457
9	42.813636	36.09951
10	42.851139	36.21101
11	42.887451	36.323356
12	42.925537	36.434604
13	42.960388	36.540924
14	42.995098	36.645301
15	43.035087	36.765087
16	43.073787	36.882984
17	43.10337	36.974617

Table 2

Phase	**Number Picks**	**Chi Squared**	**RMS Misfit (s)**
PprP	866	3.442881645	0.129567735
Pg	5334	2.038537344	0.106868266
PmP	1502	2.182268919	0.182210481
Pn	249	2.604642144	0.200007259

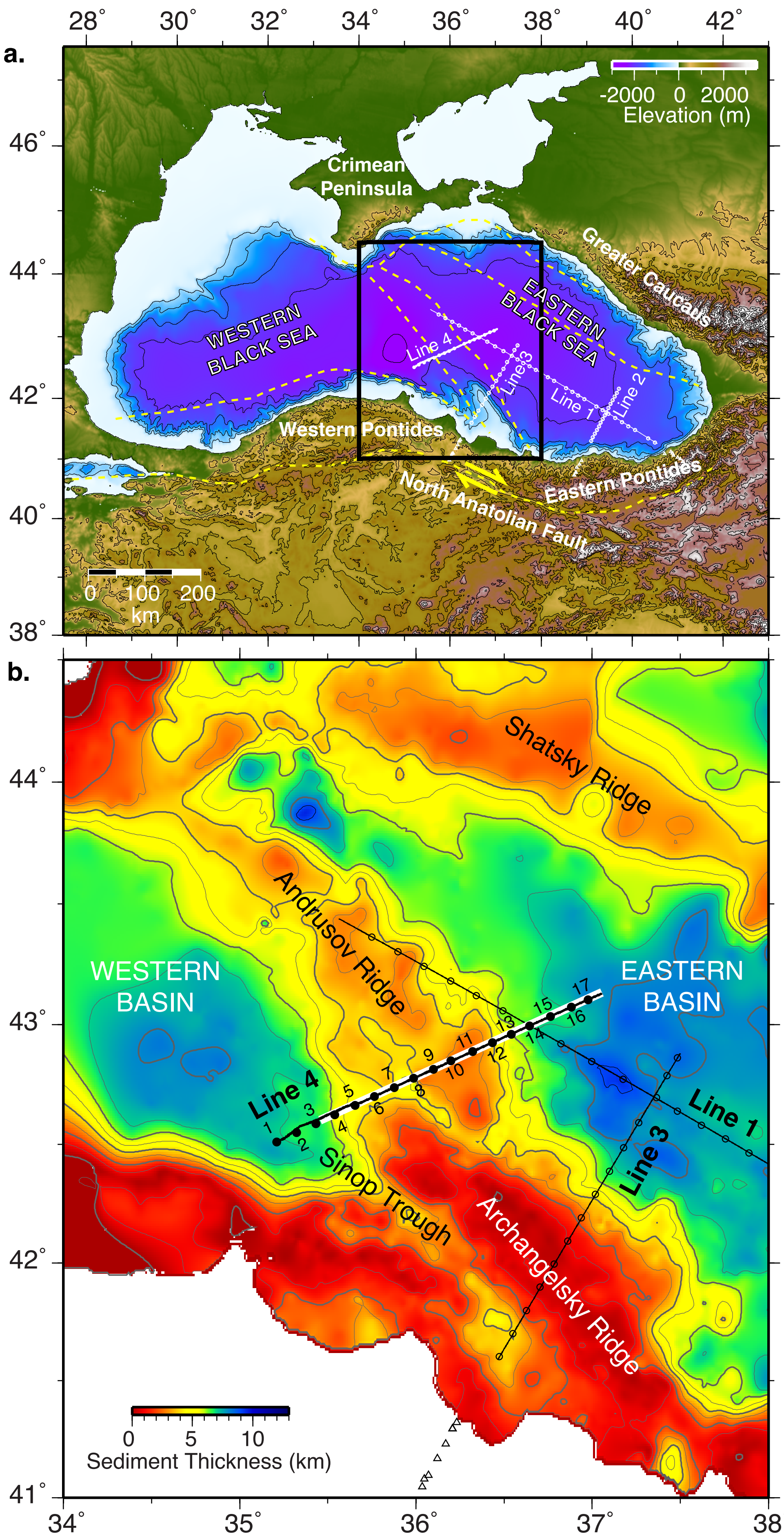
a.
28° 30° 32° 34° 36° 38° 40° 42°
46° 44° 42° 40° 38°
-2000 0 2000
Elevation (m)
Crimean Peninsula
Greater Caucasus
EASTERN BLACK SEA
WESTERN BLACK SEA
Line 4
Line 3
Line 1
Line 2
Western Pontides
Eastern Pontides
North Anatolian Fault
0 100 200
km
b.
Shatsky Ridge
Andrusov Ridge
WESTERN BASIN
EASTERN BASIN
Line 4
Line 1
Line 3
Sinop Trough
Archangelsky Ridge
0 5 10
Sediment Thickness (km)
44° 43° 42° 41°
34° 35° 36° 37° 38°

Figure 2

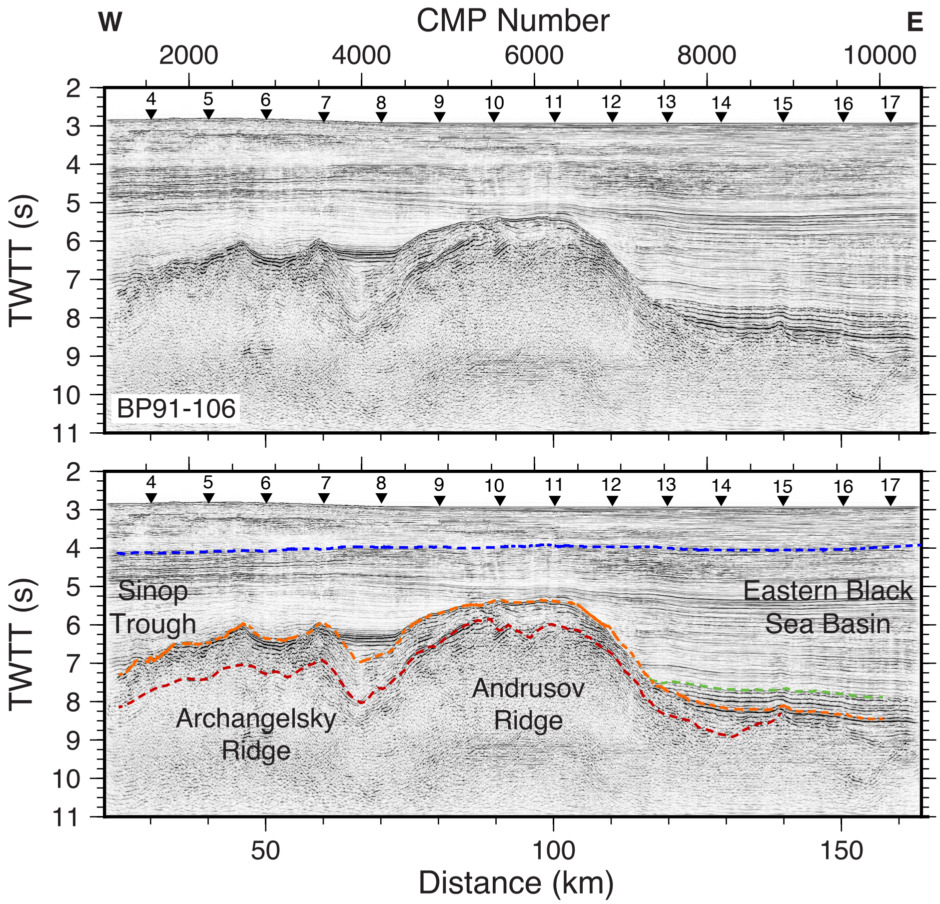
W
CMP Number
E
2000
4000
6000
8000
10000
TWTT (s)
BP91-106
Sinop
Trough
Eastern Black
Sea Basin
Archangelsky
Ridge
Andrusov
Ridge
50
100
150
Distance (km)

Figure 3

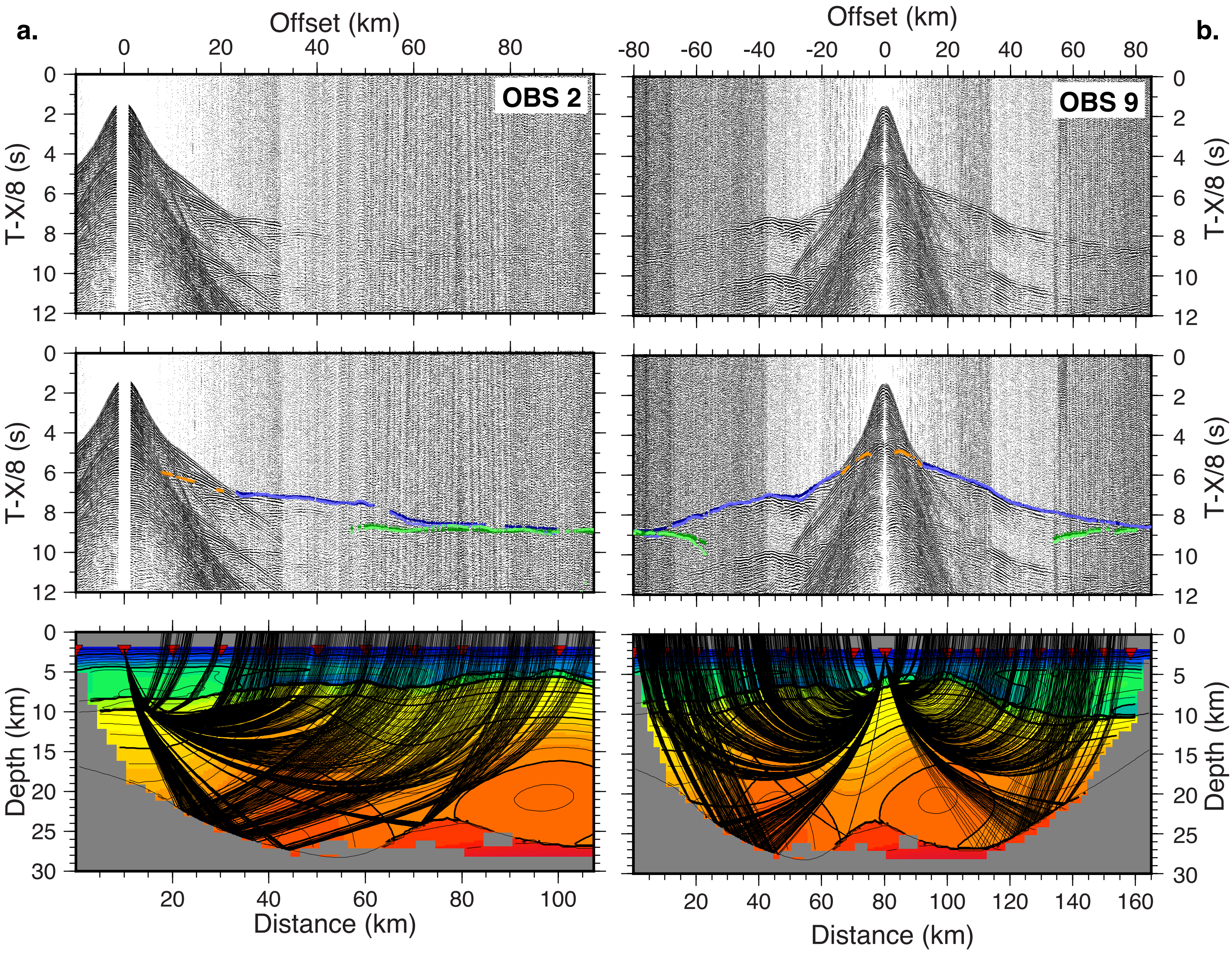

Figure 3

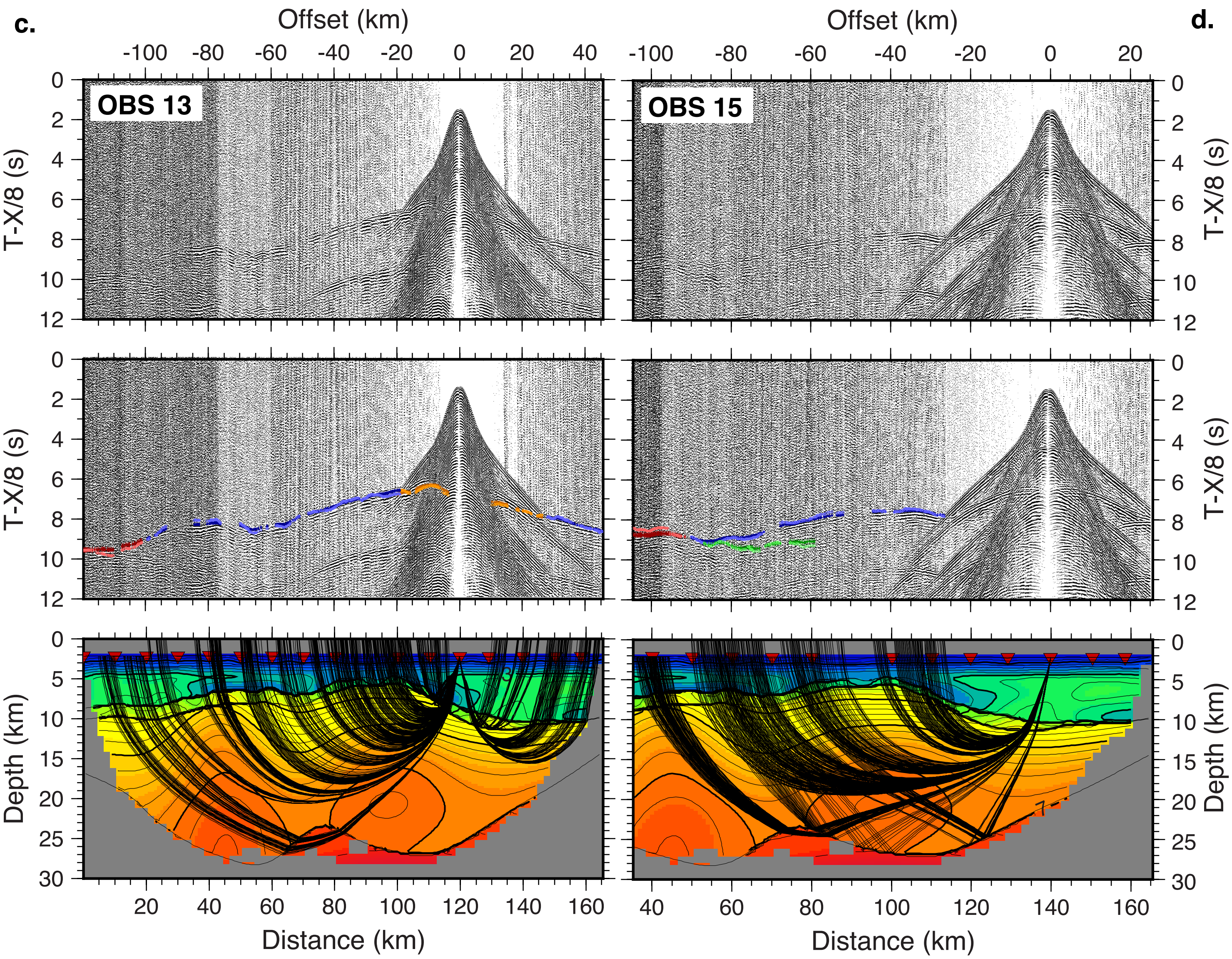

Figure 4

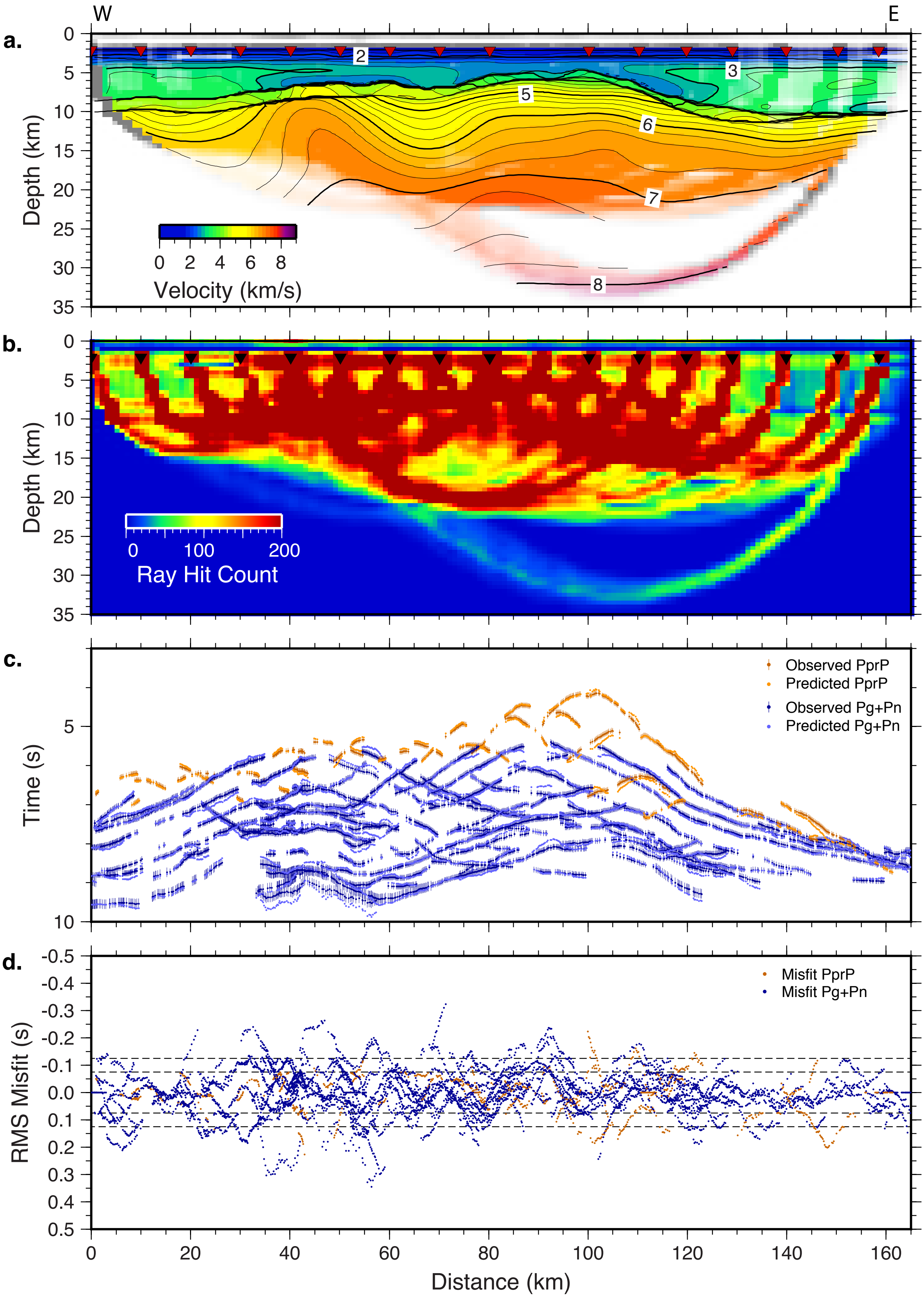
W
E
a.
b.
c.
d.
Depth (km)
Velocity (km/s)
Ray Hit Count
Time (s)
Observed PprP
Predicted PprP
Observed Pg+Pn
Predicted Pg+Pn
RMS Misfit (s)
Misfit PprP
Misfit Pg+Pn
Distance (km)

Figure 5

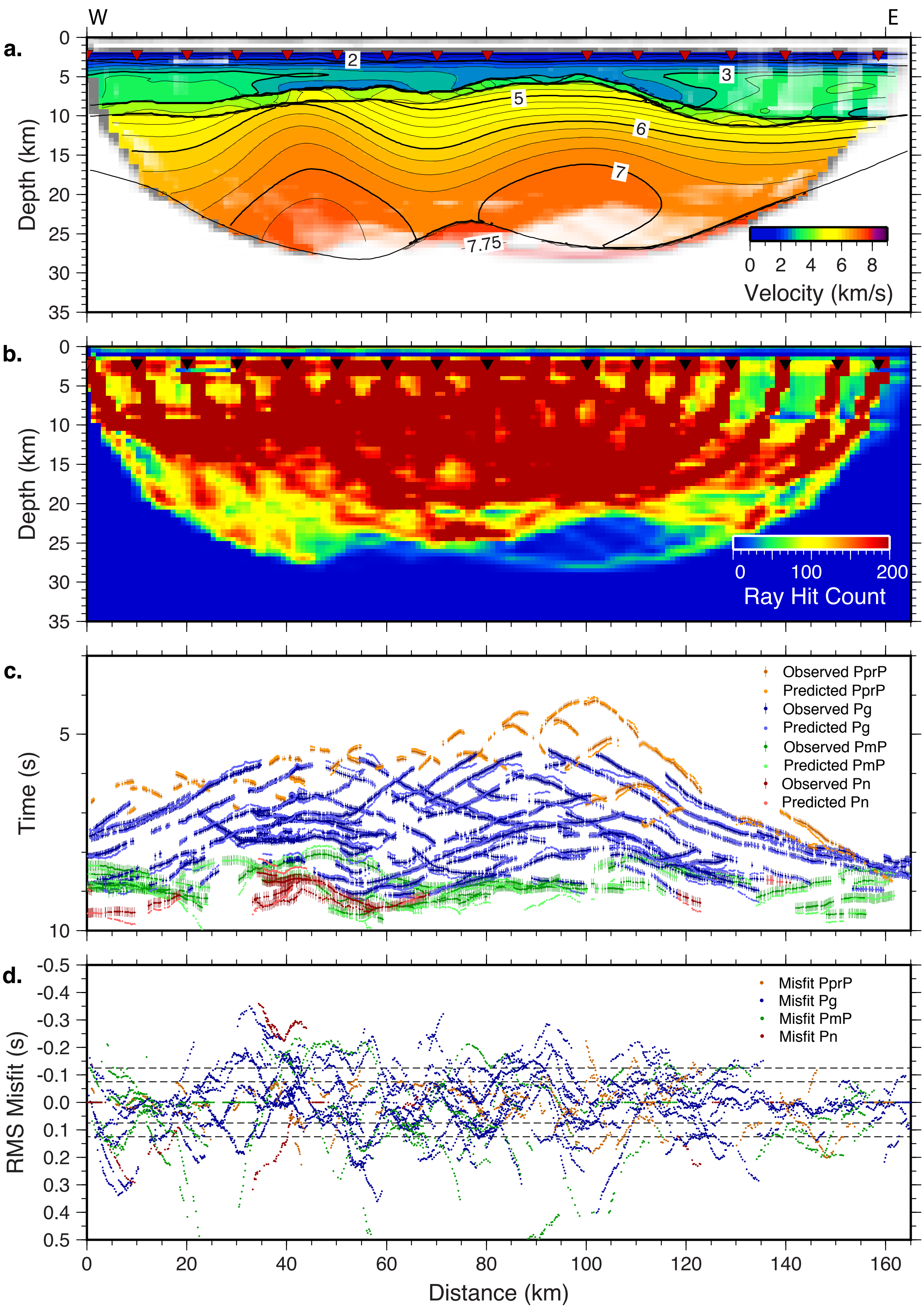

W
E
a.
Depth (km)
2
3
5
6
7
7.75
0 2 4 6 8
Velocity (km/s)
b.
Depth (km)
0 100 200
Ray Hit Count
c.
Time (s)
Observed PprP
Predicted PprP
Observed Pg
Predicted Pg
Observed PmP
Predicted PmP
Observed Pn
Predicted Pn
d.
RMS Misfit (s)
Misfit PprP
Misfit Pg
Misfit PmP
Misfit Pn
Distance (km)

Figure 6

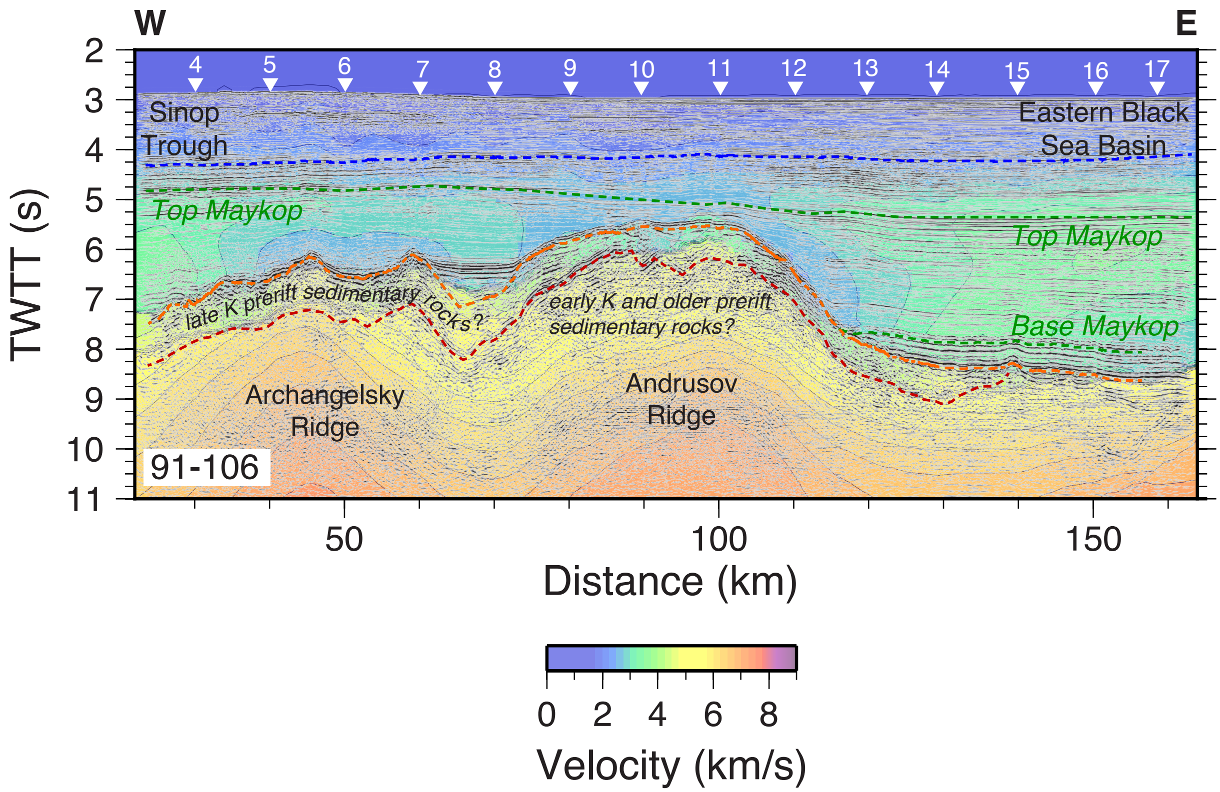

W
E
2
3
4
5
6
7
8
9
10
11
TWTT (s)
4
5
6
7
8
9
10
11
12
13
14
15
16
17
Sinop Trough
Eastern Black Sea Basin
Top Maykop
Top Maykop
Base Maykop
late K prerift sedimentary rocks?
early K and older prerift sedimentary rocks?
Archangelsky Ridge
Andrusov Ridge
91-106
50
100
150
Distance (km)
0
2
4
6
8
Velocity (km/s)

Figure 7

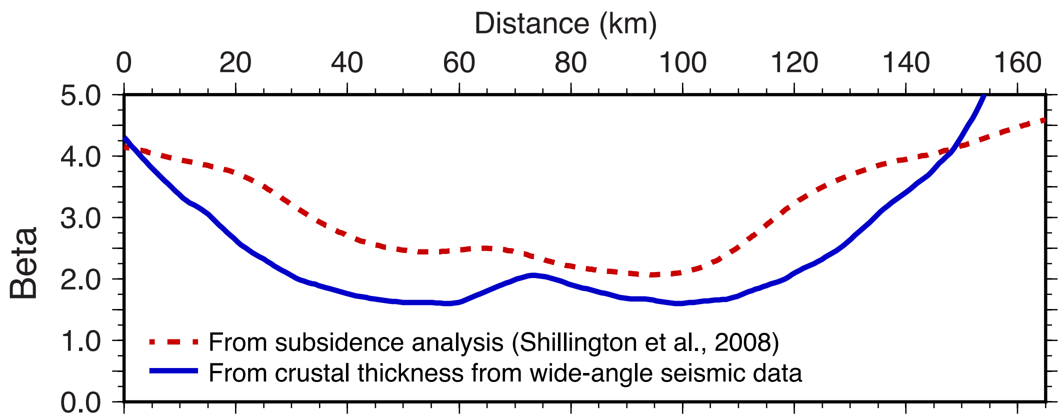
Distance (km)
0
20
40
60
80
100
120
140
160
5.0
4.0
3.0
2.0
1.0
0.0
Beta
From subsidence analysis (Shillington et al., 2008)
From crustal thickness from wide-angle seismic data